Single production of vectorlike top partner decaying to Wb in the leptonic channel at ep colliders in the littlest Higgs model with T-parity

Bingfang Yang,[1,*] Biaofeng Hou,[1,†] Huaying Zhang,[1] and Ning Liu[2]

[1]College of Physics and Materials Science, Henan Normal University, Xinxiang 453007, China
[2]Department of Physics and Institute of Theoretical Physics, Nanjing Normal University, Nanjing 210023, China

(Received 13 January 2019; published 3 May 2019)

In the littlest Higgs model with T-parity (LHT), we study the single production of a vectorlike top partner with the subsequent decay $T_+ \to Wb$ in the leptonic channel at the ep colliders. Focusing on the LHeC ($\sqrt{s} = 1.98$ TeV) and FCC-eh ($\sqrt{s} = 5.29$ TeV), we investigate the observability of the single top partner production with the unpolarized and polarized electron beams, respectively. As a result, the statistical significance can be enhanced by the polarized electron beams. Under the current constraints, the search for T_+ in the Wb channel at the LHeC cannot provide a stronger limit on the top partner mass. By contrast, the search for the T_+ in this channel at the FCC-eh with polarized e^- beams can exclude the top partner mass up to 1350 GeV, 1500 GeV, and 1565 GeV with integrated luminosities of 100 fb^{-1}, 1000 fb^{-1}, and 3000 fb^{-1} at the 2σ level, which is an improvement with respect to the current indirect searches and the LHC direct searches. Furthermore, we also give an extrapolation to the high-luminosity LHC with $\sqrt{s} = 14$ TeV and $L = 3000$ fb^{-1}. Our results show that the LHT model is still a natural solution to the shortcomings of the electroweak and scalar sector although it has been constrained severely.

DOI: 10.1103/PhysRevD.99.095002

I. INTRODUCTION

The standard model (SM) of particle physics, in particular after the discovery of the SM-like Higgs boson in 2012 [1,2], has achieved great success. However, the SM cannot describe all phenomena observed so far and still has some theoretical problems in itself. The most notable one is the hierarchy problem caused by the Higgs mass quadratic divergence [3], which has attracted a lot of attention and has been the main guideline for the possible model building of new physics beyond the SM. Among these models, the littlest Higgs model with T-parity (LHT) [4–6] is a powerful candidate.

The LHT model constructs the Higgs boson as a pseudo-Nambu-Goldstone boson and introduces the T-parity to avoid the constraint from the electroweak precision observables (EWPO). In this model, the quadratic divergence contributions to Higgs mass from the SM particles are canceled by the corresponding heavy partners. Here, an additional vectorlike top partner (T_+) with a T-even quantum number is introduced to cancel the largest contribution induced by the top quark loop. Except for the different spins, this fermionic top partner has different parities from the supersymmetric (SUSY) scalar top partner (stop) [7]; i.e., the former is T-even and the latter is R odd. So, we expect the SUSY stop searches at the LHC to have little effect on this T-even top partner searches. So far, many searches for the vectorlike top partner at the LHC have been performed by ATLAS [8] and CMS [9], and no excess above the SM expectation is observed. As a consequence, they give the strongest limits on the top partners. Meanwhile, the relevant phenomenological studies have been performed widely [10]. In the future, the LHC will be upgraded to the High Luminosity LHC (HL-LHC) with $\sqrt{s} = 14$ TeV and the integrated luminosity $L = 3000$ fb^{-1} [11]. In addition, there are other collider schemes being proposed to search for new physics, such as high energy hadron colliders: High Energy LHC (HE-LHC) [11], Future Circular Hadron Collider (FCC-hh) [12], and Super proton-proton Collider (SppC) [13], as well as lepton colliders: International Linear Collider (ILC) [14], Compact Linear Collider (CLIC) [15], and Circular Electron Positron Collider (CEPC) [13]. At these colliders, the larger events and higher accuracy will be achieved, which will provide a good opportunity for measuring the observables precisely and probing the new physics effects.

At the LHC, the dominant production modes of the top partners are pair produced, and they usually suffer from the SM top quark backgrounds. On the other hand, in view of the great achievements at the Hadron-Electron Ring Accelerator (HERA) [16], the future high-energy ep colliders will give us a whole new scene and has drawn wide attention [17]. The related physics are concerned with

*yangbingfang@htu.edu.cn
†resonhou@zknu.edu.cn

new phenomena possibly occurring in the fusion of electrons and partons at TeV energies. These colliders can provide higher collision energies than the e^+e^- colliders and cleaner environment than the pp colliders. At present, the proposed ep collider is the Large Hadron Electron Collider (LHeC) [18], which is designed to collide a 60–140 GeV electron beam with a 7 TeV proton beam from the LHC. This may later be extended to Future Circular electron-hadron Collider (FCC-eh) [19], which features a 50 TeV proton beam from the FCC-hh. Furthermore, the electron beam can be polarized and has an enormous scope to probe electroweak and Higgs physics. At this kind of colliders, the dominant production modes of the top partner will be singly produced. In this paper, we will study the observability of the single top partner production at the ep colliders in the LHT model.

The structure of the paper is as follows: In Sec. II, we briefly review the top partner in the LHT model. In Sec. III, we study the single production of top partner T_+ followed by Wb in the leptonic channel at the ep colliders including the LHeC and FCC-eh. Finally, we give a short summary in Sec. IV.

II. TOP PARTNER IN THE LHT MODEL

In this section, we will briefly review the LHT model; the details of the model and phenomenology can be found in Ref. [20]. This model is based on a $SU(5)/SO(5)$ nonlinear sigma model. At scale $f \sim \mathcal{O}(\mathrm{TeV})$, the global symmetry $SU(5)$ is broken down to $SO(5)$ by the vacuum expectation value (VEV) of the Σ field,

$$\Sigma_0 = \begin{pmatrix} & & \mathbf{1}_{2\times 2} \\ & 1 & \\ \mathbf{1}_{2\times 2} & & \end{pmatrix}. \tag{1}$$

The gauge group is assigned to be the subgroup of $SU(5)$ as $G_1 \times G_2 = [SU(2) \times U(1)]_1 \times [SU(2) \times U(1)]_2$, which is broken down to the diagonal SM electroweak gauge group $SU(2)_L \times U(1)_Y$ by the coincident VEV in Eq. (1). After the symmetry breaking, there arise four new heavy gauge bosons $W_H^{\pm}, Z_H, A_H$ whose masses are given at $\mathcal{O}(v^2/f^2)$ by

$$M_{W_H} = M_{Z_H} = gf\left(1 - \frac{v^2}{8f^2}\right), \qquad M_{A_H} = \frac{g'f}{\sqrt{5}}\left(1 - \frac{5v^2}{8f^2}\right), \tag{2}$$

with g and g' being the SM $SU(2)_L$ and $U(1)_Y$ gauge couplings, respectively. The lightest T-odd particle A_H can serve as a candidate for dark matter (DM). Note that the VEV v needs to be redefined as

$$v = \frac{f}{\sqrt{2}}\arccos\left(1 - \frac{v_{\mathrm{SM}}^2}{f^2}\right) \simeq v_{\mathrm{SM}}\left(1 + \frac{1}{12}\frac{v_{\mathrm{SM}}^2}{f^2}\right), \tag{3}$$

where $v_{\mathrm{SM}} = 246$ GeV is the SM Higgs VEV.

In order to avoid the strong constraints from the EWPO, a feasible way is to impose a discrete symmetry called T-parity in this model, which plays a similar role as R-parity in SUSY. Apart from the scalar and gauge sectors, the T-parity also has to be implemented in the fermion sector so that every SM fermion has a mirror partner with a T-odd quantum number.

In the top quark sector, an additional vectorlike T-even top partner T_+ is introduced for canceling the large one-loop quadratic divergences of Higgs mass caused by the top quark. Then, the implementation of T-parity also requires its own T-odd mirror partner T_-. The top quark has to be represented as an incomplete $SU(5)$ multiplet Q_1 and its T-parity partner Q_2,

$$Q_1 = \begin{pmatrix} \psi_1 \\ t'_1 \\ \mathbf{0} \end{pmatrix} \qquad Q_2 = \begin{pmatrix} \mathbf{0} \\ t'_2 \\ \psi_2 \end{pmatrix}, \tag{4}$$

which are related via

$$Q_1 \overset{T}{\leftrightarrow} -\Sigma_0 Q_2, \quad \text{with} \quad \psi_i = -i\sigma_2 \begin{pmatrix} t_i \\ b_i \end{pmatrix}. \tag{5}$$

Then, the T-parity invariant Lagrangian related to the top quark Yukawa interaction is given by

$$\begin{aligned} \mathcal{L}_{\mathrm{top}} = & -\frac{\lambda_1 f}{2\sqrt{2}}\epsilon_{ijk}\epsilon_{xy}[(\overline{Q_1})_i \Sigma_{jx}\Sigma_{ky} - (\overline{Q_2}\Sigma_0)_i \tilde{\Sigma}_{jx}\tilde{\Sigma}_{ky}]u_R^3 \\ & - \lambda_2 f(\bar{t}'_1 t'_{1R} + \bar{t}'_2 t'_{2R}) + \mathrm{H.c.}, \end{aligned} \tag{6}$$

where λ_1 and λ_2 are two dimensionless top-quark Yukawa couplings, ϵ_{ijk} and ϵ_{xy} are the antisymmetric tensors with i, j, $k = 1, 2, 3$ and x, $y = 4, 5$, and

$$\tilde{\Sigma} \equiv T[\Sigma] = \Sigma_0 \Omega \Sigma^{\dagger} \Omega \Sigma_0, \ \text{with} \ \Omega = \mathrm{diag}(1,1,-1,1,1). \tag{7}$$

After the symmetry breaking, we can get the masses of top quark and its partners from the Lagrangian in Eq. (6) and parametrize them at $\mathcal{O}(v^2/f^2)$ in the following form:

$$\begin{aligned} m_t &= \frac{\lambda_2 vR}{\sqrt{1+R^2}}\left[1 + \frac{v^2}{f^2}\left(-\frac{1}{3} + \frac{1}{2}\frac{R^2}{(1+R^2)^2}\right)\right] \\ m_{T_+} &= \frac{f}{v}\frac{m_t(1+R^2)}{R}\left[1 + \frac{v^2}{f^2}\left(\frac{1}{3} - \frac{R^2}{(1+R^2)^2}\right)\right] \\ m_{T_-} &= \frac{f}{v}\frac{m_t\sqrt{1+R^2}}{R}\left[1 + \frac{v^2}{f^2}\left(\frac{1}{3} - \frac{1}{2}\frac{R^2}{(1+R^2)^2}\right)\right], \end{aligned} \tag{8}$$

where R is defined as $R = \lambda_1/\lambda_2$.

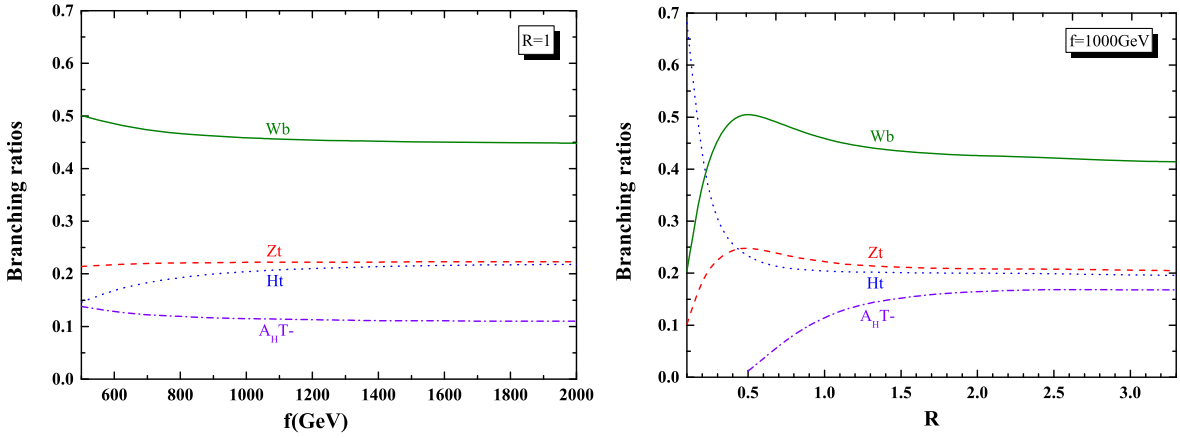

FIG. 1. The branching ratios of T_+ as a function of the scale f for $R = 1$ (left) and as a function of the ratio R for $f = 1000$ GeV (right).

Due to the conservation of T parity, the vectorlike top partner T_+ is the only new particle that can be singly produced, which means all other new particles have to be pair produced in this model. Apart from the usual decay channels: $T_+ \to bW^+$, $T_+ \to tZ$, and $T_+ \to th$, the T_+ has an additional decay channel $T_+ \to T\_A_H$ so that it has richer phenomenology. For clarity, we show the branching ratios of these four decay channels as a function of the scale f (left) and as a function of the ratio R (right) in Fig. 1. We can see that the additional decay channel $T_+ \to T\_A_H$ has a weak dependence on the scale f and is mainly determined by the ratio R. It is kinematically opened only for $R > 0.5$ when $f = 1000$ GeV and will help to detect the effect of the LHT model.

Now, let us go back to the fine-tuning problem, which is the initial driving force of the LHT model. The fine-tuning problem can be quantified by the definition in Ref. [21]; the form of the fine-tuning measure is the ratio of the experimentally measured Higgs mass squared parameter ($\mu^2_{\rm obs} = m_h^2/2$) and the absolute value of the radiative corrections from the top partners to the Higgs quadratic operator ($\delta\mu^2$),

$$\Delta = \frac{\mu^2_{\rm obs}}{|\delta\mu^2|}, \qquad \delta\mu^2 = -\frac{3\lambda_t m^2_{T_+}}{8\pi^2}\log\frac{\Lambda}{m^2_{T_+}}. \tag{9}$$

Here λ_t is the SM top Yukawa coupling and $\Lambda = 4\pi f$ is the cutoff scale of the LHT model. According to this definition, a smaller value means a severer fine-tuning.

III. SINGLE TOP PARTNER PRODUCTION AT THE *ep* COLLIDERS

At the ep colliders, the dominant way to produce the T_+ is through the t channel by exchanging a W boson, as shown in Fig. 2. The new coupling vertex T_+Wb related to this process is given by

$$\bar{T}_+ W^{+\mu} b: \ \frac{ig}{\sqrt{2}}(V_{\rm CKM})_{tb}\frac{R^2}{1+R^2}\frac{v}{f}\left[1+\frac{v^2}{f^2}d_2\right]\gamma^\mu P_L \tag{10}$$

$$\text{with: } d_2 = -\frac{5}{6}+\frac{1}{2}\left(\frac{R}{1+R^2}\right)^2(R^2+4), \tag{11}$$

where P_L is the chiral projection operator and $(V_{\rm CKM})_{tb}$ is one of the CKM elements. The $(V_{\rm CKM})_{tb}$ will not be a unit if one assumes that there is minimal flavor violation in the LHT model [22]. Here, we set $(V_{\rm CKM})_{tb} = 1$.

This process depends only on two free parameters closely related to the T_+, that is the scale f and the ratio R. In our previous work [23], we have considered the limits on the LHT model from the dark matter direct detections including LUX, PandaX-II, and XENON1T. In order to produce the correct relic abundance, it requires the heavy photon A_H to coannihilate with the light mirror quarks or mirror leptons, which leads the Yukawa coupling κ of the mirror fermions to be confined in a small region and causes the LHT model to become unnatural. Besides, the A_H will no longer serve as a dark matter candidate in the case of T-parity violation by instantons. Considering the current constraints [24,25], we take the loose parameter space and allow the scale f to be as low as 500 GeV, and the range of the ratio R is chosen as $R \in [0.1, 3.3]$. The relevant SM input parameters are taken as follows [26]:

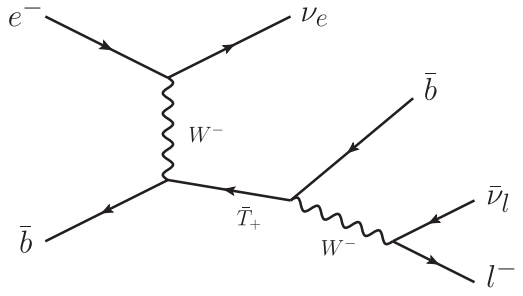

FIG. 2. Single top partner production and decay to Wb channel at the ep collision.

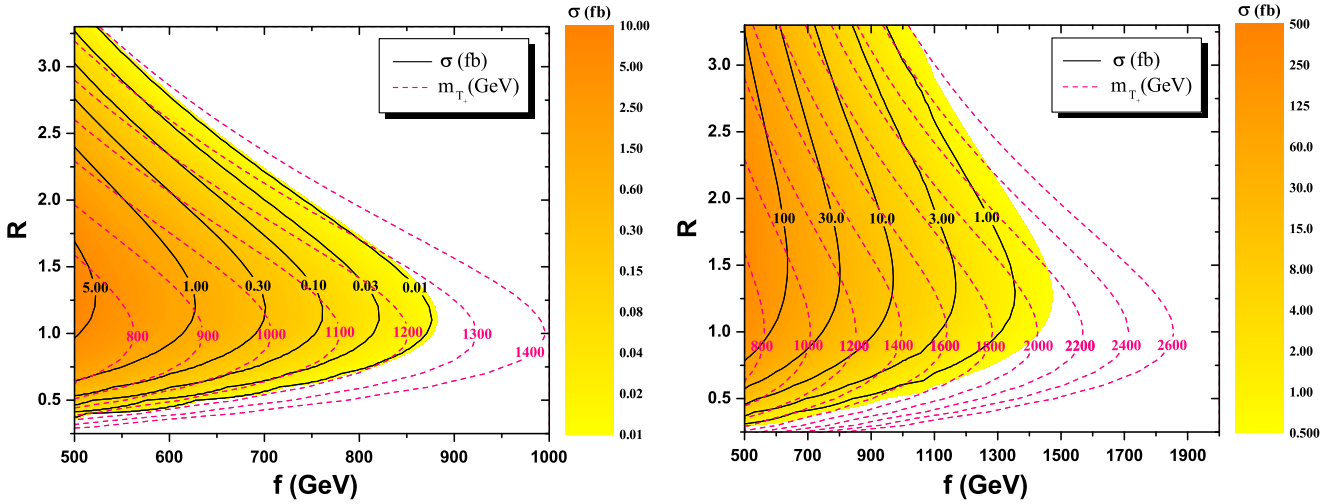

(a) LHeC (unPola) (b) FCC-eh (unPola)

FIG. 3. The unpolarized cross section $\sigma(e^- p \to \nu_e \bar{T}_+)$ distribution in the R–f plane at LHeC (a) and FCC-eh (b).

$$m_t = 173.0\,\text{GeV}, \quad m_Z = 91.1876\,\text{GeV}, \quad m_h = 125.0\,\text{GeV},$$
$$\sin^2\theta_W = 0.231, \quad \alpha(m_Z) = 1/128.$$

For the collision energy, we choose 140 GeV × 7 TeV and 140 GeV × 50 TeV as the e^- and p beam energies, which correspond to LHeC ($\sqrt{s} = 1.98$ TeV) and FCC-eh ($\sqrt{s} = 5.29$ TeV), respectively. Then, we scan the parameter space with the package EasyscanHEP [27] and show the unpolarized cross sections of single T_+ production at the LHeC [Fig. 3(a)] and FCC-eh [Fig. 3(b)] in the R–f plane. We can see that the cross sections almost coincide with the curves of T_+ mass and decrease rapidly with the increase of this mass. Due to the larger center-of-mass energy, the cross section at the FCC-eh can be enhanced greatly compared to the LHeC.

As we know, the SM predicts that only the left-handed electrons participate in the charged current. So it will be helpful to consider the polarized e^- beams at the ep colliders. In analogy with Eq. (1.15) in Ref. [28], the cross section of this process with longitudinally polarized e^- beams and unpolarized proton beams can be expressed as

$$\sigma_{\text{pola}} \propto (1 - P_{e^-})\sigma_L, \tag{12}$$

where σ_L is the cross section for completely left-handed polarized e^- beams ($P_{e^-} = -100\%$). Thus, the ratio of the polarized cross section to the unpolarized one can be written as

$$R_\sigma \equiv \frac{\sigma_{\text{pola}}}{\sigma_{\text{unpola}}} = 1 - P_{e^-}. \tag{13}$$

We can see that the ratios R_σ are independent of the top partner mass m_{T_+}. In the following calculation, we take $P_{e^-} = -80\%$ as a reasonable polarization degree so that the polarized beams can enhance the cross sections effectively.

Considering the larger cross section, we will concentrate on the Wb channel in this work. The complete production and decay chain is shown in Fig. 2,

$$e^- p \to \nu_e \bar{T}_+ (\to \bar{b} W^-) \to \nu_e (\bar{b} \nu_l l^-) \to l^- + \bar{b} + \not{E}_T.$$

We can see that the signal of final states is mainly composed of one charged lepton, one b jet, and missing energy. The dominant SM backgrounds come from the following four processes:

(i) background $t\nu$: $e^- p \to \bar{t}(\to \bar{b} W^-)\nu_e \to l^- + \bar{b} + \not{E}_T$
(ii) background $Wb\nu$: $e^- p \to W^-(\to l^- \bar{\nu}_l)\bar{b}\nu_e \to l^- + \bar{b} + \not{E}_T$
(iii) background eZb: $e^- p \to e^- Z(\to \nu_l \bar{\nu}_l) b(\bar{b}) \to e^- + b(\bar{b}) + \not{E}_T$
(iv) background $tZ\nu$: $e^- p \to \bar{t}(\to \bar{b} l^- \bar{\nu}_l) Z(\to \nu_l \bar{\nu}_l)\nu_l \to l^- + \bar{b} + \not{E}_T$,

where the SM top quark is on shell produced in the background $t\nu$ and this process is not included in the background $Wb\nu$.

In this work, the calculation of cross sections and generation of signal/background events are both performed by using MadGraph5_aMC@NLO(MG5) [29] with the parton distribution function (PDF) NNPDF23 [30], where the decay width of T_+ is generated by MG5 automatically. Meanwhile, the Monte Carlo (MC) generator level cuts are selected as follows:

$$\Delta R(i,j) > 0.4, \qquad i,j = l,j$$
$$p_T^l > 10\ \text{GeV}, \qquad |\eta^l| < 5$$
$$p_T^j > 20\ \text{GeV}, \qquad |\eta^j| < 5,$$

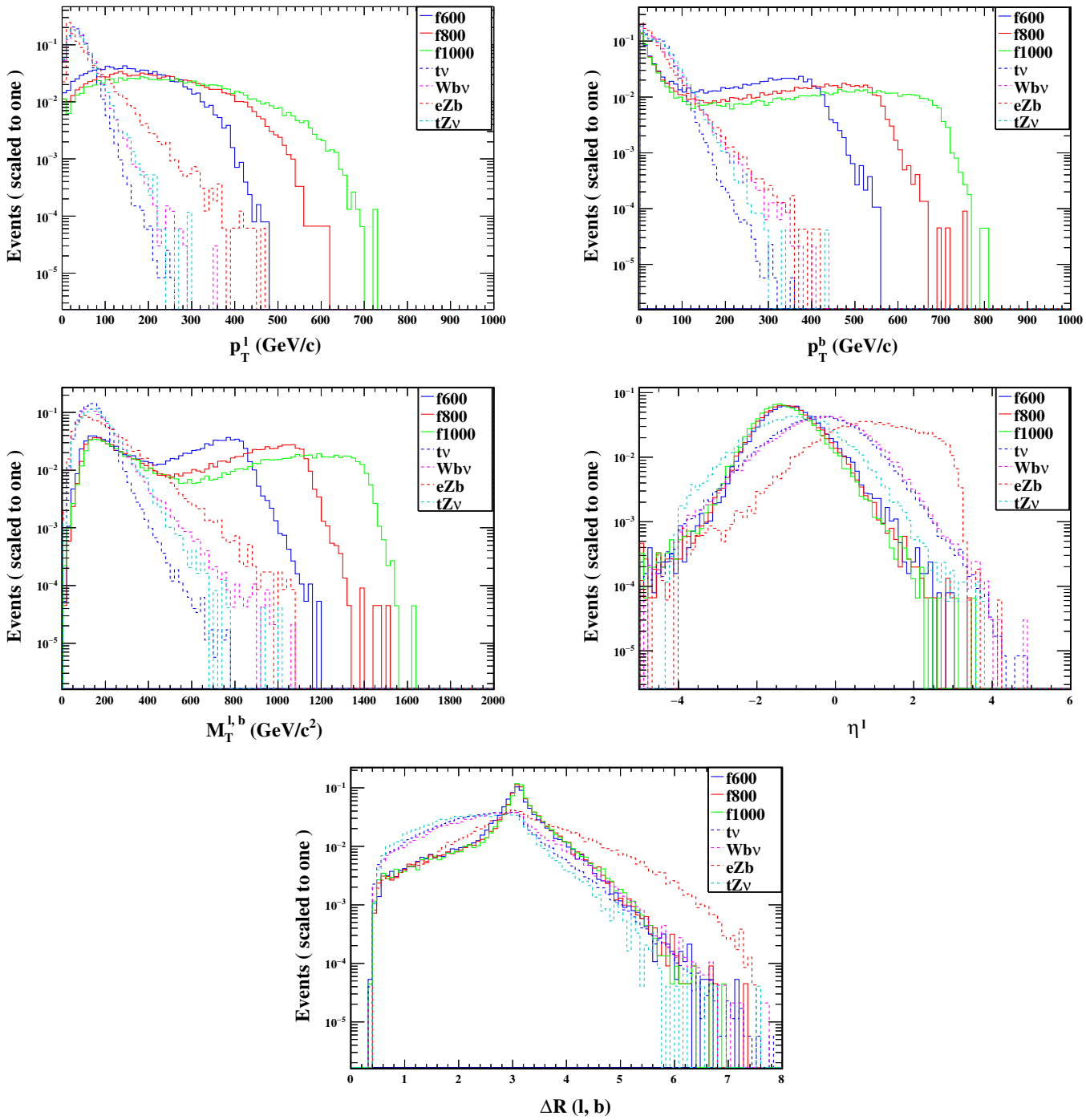

FIG. 4. The normalized distributions of $p_T^l, p_T^b, \eta^l, M_T^{l,b}$, and $\Delta R(l,b)$ for signals and backgrounds at LHeC with unpolarized e^- beams.

where $\Delta R(i,j) = \sqrt{(\Delta\phi)^2 + (\Delta\eta)^2}$ with $\Delta\phi$ the difference of azimuthal angle between object i and j, meanwhile $\Delta\eta$ the difference of pseudorapidity between them.

Next, we let the parton-level events go through the PYTHIA [31] for the parton shower and hadronization. Then the Delphes [32] is used for the fast detector simulation, where the $anti-k_t$ algorithm [33] in the delphes card of the FCC-eh collider is chosen for clustering the jets with the distance parameter $\Delta R = 0.4$. Finally, the reconstructed-level events derived from the above process are used to do the kinematic and cut-based analysis by MadAnalysis5 [34].

TABLE I. Cut flows of the signals and backgrounds at LHeC with unpolarized (in parenthesis) and polarized e^- beams for the three signal benchmark points $m_{T_+} \approx 840, 1120, 1400$ GeV.

	Signal ($\times 10^{-3}$ fb)			Background ($\times 10^{-3}$ fb)			
	840 GeV	1120 GeV	1400 GeV	$t\nu$	$Wb\nu$	eZb	$tZ\nu$
Basic cuts	(129) 232	(5.04) 9.05	(0.095) 0.170	(1.20E6) 2.17E6	(18378) 33081	(1557) 2272	(516) 928
Cut1	(85) 154	(3.32) 5.95	(0.061) 0.110	(7.46E5) 1.34E6	(11140) 19979	(930) 1375	(328) 592
Cut2	(49) 89	(2.23) 3.95	(0.043) 0.077	(124) 305	(34) 71	(9) 14	(0.44) 0.69
Cut3	(49) 89	(2.23) 3.95	(0.043) 0.077	(118) 282	(31) 62	(8) 13	(0.40) 0.69
Cut4	(42) 77	(1.96) 3.45	(0.038) 0.068	(6) 6	(19) 42	(7) 12	(0) 0
Cut5	(39) 71	(1.81) 3.19	(0.035) 0.063	(6) 6	(12) 23	(4) 5	(0) 0
Total eff.	(30.2%) 30.4%	(35.8%) 35.3%	(37.1%) 37.2%	(5.17E-6) 2.68E-6	(6.38E-4) 6.94E-4	(0.23%) 0.24%	(0) 0

A. Detection at LHeC with $\sqrt{s} = 1.98$ TeV

In this section, we will use MC simulation to analyze the detection sensitivity of the single T_+ production at the LHeC through the channel as shown in Fig. 2.

Considering the blurring effect of the detector, we require that the signal contains one charged lepton (only for e, μ) and at least one b jet. In order to suppress the background more effectively, some other cuts need to be taken. Since the signal leptons and b quarks are derived from the decay of a heavy top partners, they should have a large transverse momentum and ΔR. In addition, the signal transverse mass, obtained from a system comprised of the lepton, b quark, and the invisible transverse momentum of the event [35], should have a peak around the T_+ mass. Besides, due to the asymmetry of initial beam energies, the pseudorapidity will be a very good observable to distinguish the leptons whether they come from the scattering of initial states or not. Here, we take the electron beam along the positive direction of the z axis and the proton beam along the opposite direction. This will lead the pseudorapidity of most final electrons from the scattering of initial states to positive values and most final leptons from the decay of heavy particles to negative values due to the motion of the center of mass system caused by the large proton momentum. The normalized distributions of these observables are shown in Fig. 4 for three benchmark points $f = 600$, 800, 1000 GeV and $R = 1$ (corresponding to $m_{T_+} \approx 840, 1120, 1400$ GeV). We find that these distributions for polarized e^- beams are roughly the same as the unpolarized ones, so only take the unpolarized case, for example. According to the above analysis, we choose the specific analysis cuts as follows:

(i) cut1: $N(l) = 1, N(b) \geq 1$
(ii) cut2: $p_T^l \geq 60$ GeV, $p_T^b \geq 200$ GeV
(iii) cut3: $M_T^{l,b} \geq 450$ GeV
(iv) cut4: $\eta^l < -0.5$
(v) cut5: $\Delta R(l, b) \geq 2.0$.

We summarize the cut flows of the signals and backgrounds for unpolarized (in parenthesis) and polarized cases at LHeC in Table I, in which the cross sections (in units of 10^{-3} fb) can be understood as the event number with $L = 1000$ fb^{-1} of the signals and the backgrounds. We can find that the polarized cross section is about 1.8 times larger than the unpolarized case. After imposing the above selection cuts, we can see that the relevant backgrounds are suppressed effectively while the signal still have a relatively good efficiency. For the three benchmarks, the cut efficiencies can reach (30.2%) 30.4%, (35.8%) 35.3%, and (37.1%) 37.2% for the (un)polarized case, respectively. In the next calculation, we will choose the conservative cut efficiency (30.2%) 30.4% for all the (un) polarized signal parameter points.

The statistical significance (SS) can be evaluated after the final cut by using the Poisson formula [36],

$$SS = \sqrt{2L\left[(\sigma_S + \sigma_B)\ln\left(1 + \frac{\sigma_S}{\sigma_B}\right) - \sigma_S\right]}, \quad (14)$$

where L is the integrated luminosity and σ_S, σ_B are the effective cross sections after selection cuts for signal and background, respectively.

We show the 2σ exclusion limit contour in $R - f$ plane at the LHeC with unpolarized(a) and polarized(b) e^- beams in Fig. 5 and find that the polarized e^- beam can test larger parameter space. Furthermore, the polarization of initial electron beams can still improve the SS although both the cross sections of signal and backgrounds are increased synchronously. So, we will focus on the polarized case to study the observability of the signal. In Fig. 5, we also provide the corresponding m_{T_+} contours indicated by the red dashed lines. According to the different integrated luminosities, the relevant contour regions associated with the $R - f$ plane will be detected or excluded. In order to provide more information, we also show the 2σ, 3σ, 5σ samples in the $L - m_{T_+}$ plane at the LHeC with polarized e^- beams in the left panel of Fig. 6.

In principle, we have to consider the limits on the LHT model from the indirect measurements. In our previous paper [37], the global fit of the EWPO and the latest Higgs

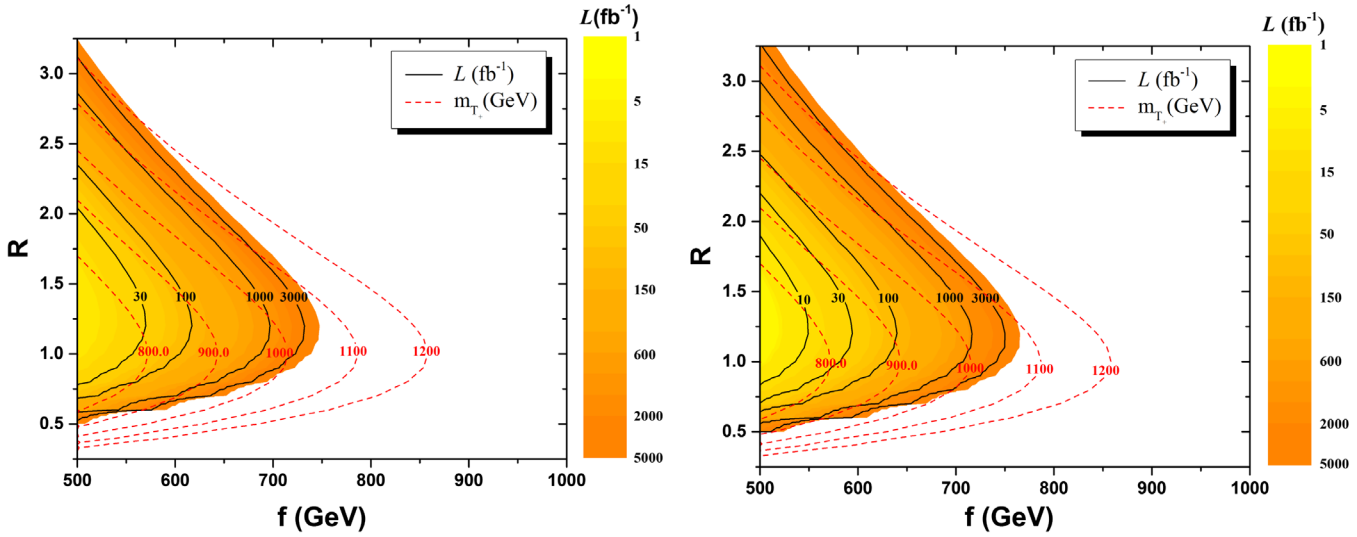

(a) LHeC (unPola) (b) LHeC (Pola)

FIG. 5. 2σ exclusion limit in $R-f$ plane at the LHeC with unpolarized e^- beams (a) and polarized e^- beams (b) for $\sqrt{s}=1.98$ TeV.

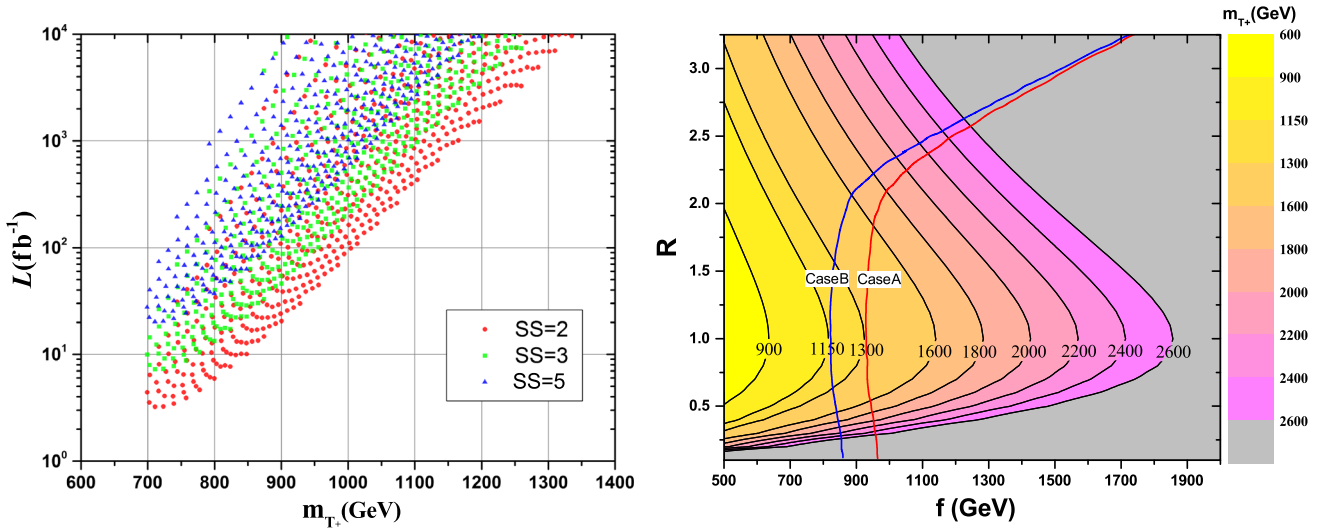

FIG. 6. (left) 2σ, 3σ, 5σ samples in $L-m_{T_+}$ plane at the LHeC with polarized e^- beams; (right) 2σ limits from EWPO and Higgs data on the m_{T_+} in the $R-f$ plane for case A and case B.

data have been performed. We show the 2σ exclusion limits on the T_+ mass in the right panel of Fig. 6, where the T_+ mass can be excluded up to 1300 (1150) GeV for case A (B). The case A and case B denote two possible ways to construct the T-invariant Yukawa interactions of the down-type quarks and charged leptons [38], which do not differ in the LHT collider phenomenology related to our work. Since the lower limit on m_{T_+} in case B is weaker than that in case A, we will focus on case A in the following discussions. Even if the high luminosities ($L=1$ ab$^{-1}\sim 5$ ab^{-1}) are used, we can see that the limit from the LHeC search for the T_+ in this Wb channel is still weaker than the current limit from the indirect measurements, i.e., the global fit of the EWPO and the latest Higgs data.

B. Detection at FCC-eh with $\sqrt{s}=5.29$ TeV

In this section, we investigate the observability of single T_+ production at the FCC-eh with $\sqrt{s}=5.29$ TeV in a similar approach as the previous section. To execute the cut-based analysis, we show the same normalized kinematic distributions for the three benchmarks ($f=600$, 800, 1000 GeV and $R=1$) in Fig. 7. We can see that the distributions involving momentum show slight overall

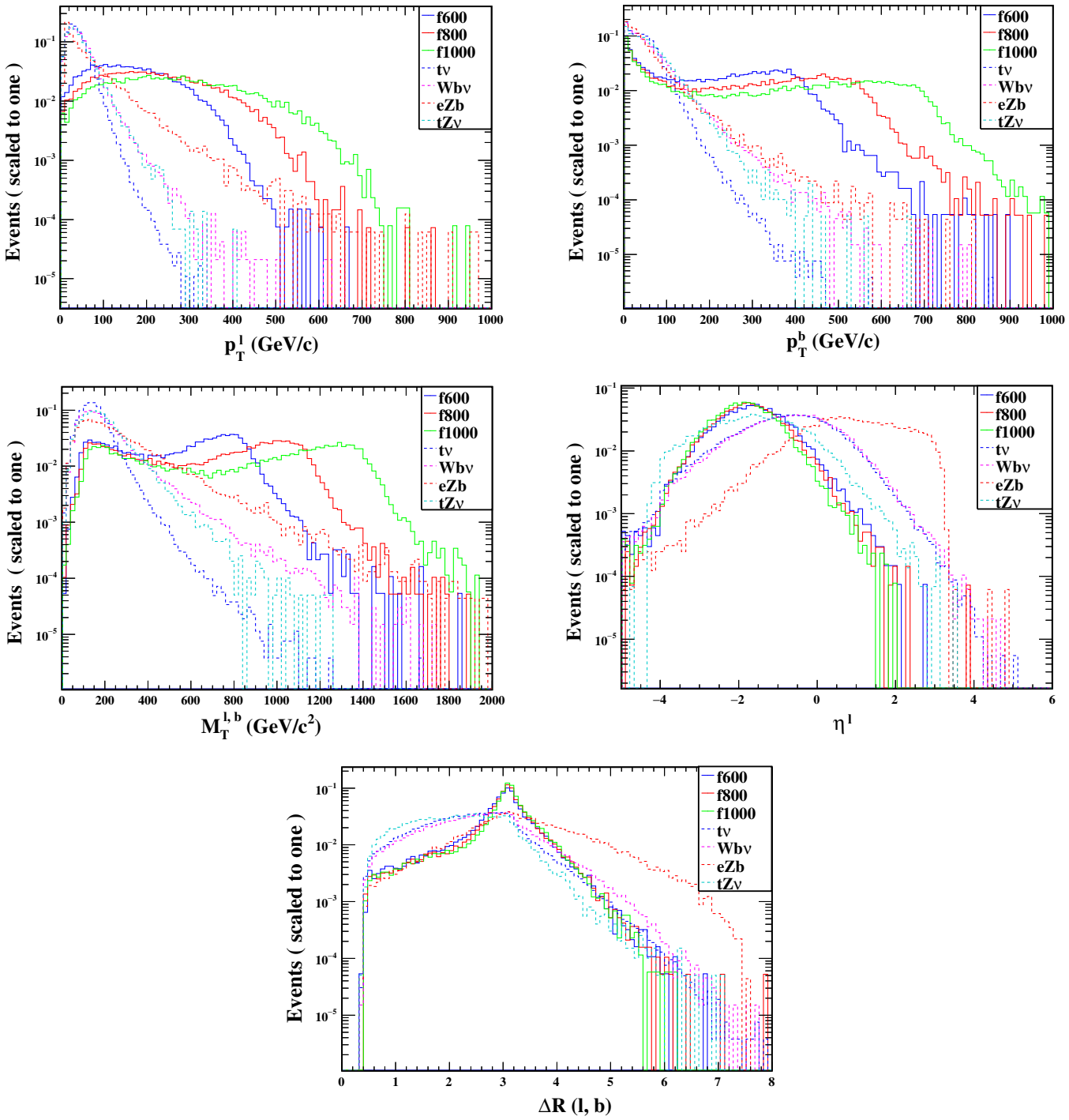

FIG. 7. Same as Fig. 4, but for FCC-eh.

rightward shifts compared to the LHeC case, which changes the cut efficiencies almost negligibly. So we choose the same cuts as in Sec. III (A), and the cut flows of the signals and backgrounds for unpolarized and polarized cases are shown in Table II. Here, the cut efficiencies of the (un)polarized case can reach (31.9%) 32.4%, (38.4%) 38.7%, and (41.3%) 41.0% for three signal benchmark points, respectively. Meanwhile, the backgrounds are suppressed effectively. Likewise, we will choose the conservative cut efficiency (31.9%) 32.4% for all the (un)polarized signal parameter points.

In Fig. 8, we show the 2σ exclusion limit contour in the $R-f$ plane at the FCC-eh with unpolarized(a) and polarized(b) e^- beams. From Fig. 8, we can see that the detected region at the FCC-eh is enlarged obviously with respect to the LHeC.

TABLE II. Cut flows of the signal and backgrounds at FCC-eh with unpolarized (in parentheses) and polarized e^- beam for the three signal benchmark points $m_{T_+} \approx 840, 1120, 1400$ GeV.

	Signal ($\times 10^{-3}$ fb)			Background ($\times 10^{-3}$ fb)			
	840 GeV	1120 GeV	1400 GeV	$t\nu$	$Wb\nu$	eZb	$tZ\nu$
Basic cuts	(8843) 1.59E4	(2086) 3754	(590) 1059	(7.05E6) 1.27E7	(1.17E5) 2.11E5	(9123) 1.35E4	(6695) 1.20E4
Cut1	(5489) 9956	(1303) 2329	(366) 652	(4.29E6) 7.72E6	(6.90E4) 1.24E5	(5464) 8216	(3737) 6727
Cut2	(3315) 6100	(920) 1658	(277) 494	(5171) 9340	(882) 1662	(189) 333	(25) 30
Cut3	(3294) 6048	(915) 1652	(276) 492	(4627) 8612	(820) 1538	(183) 326	(24) 28
Cut4	(2918) 5346	(822) 1487	(249) 444	(118) 465	(545) 1038	(164) 287	(0.26) 1
Cut5	(2825) 5154	(801) 1453	(244) 435	(94) 464	(373) 754	(78) 144	(0.26) 1
Total eff.	(31.9%) 32.4%	(38.4%) 38.7%	(41.3%) 41.0%	(1.33E-5) 3.66E-5	(0.32%) 0.36%	(0.85%) 1.06%	(3.85E-5) 7.69E-5

Recently, the limits on the LHT model from the LHC experiments have been performed in Ref. [25], where all the LHC available Run-II data at 8 and 13 TeV for searches for physics beyond the SM have been exploited and an extrapolation to the HL-LHC at 14 TeV has also been given. According to their conclusions, the minimum value of the scale f allowed by the LHC-13 TeV experiment is 950 GeV with fixed value $R = 1$ at 2σ confidence level, which corresponds to the top partner mass limit $m_{T_+} \geq 1336$ GeV. For the HL-LHC case, the minimum value of the scale f allowed is 1500 GeV with a fixed value $R = 1$ at 2σ confidence level, which corresponds to the top partner mass limit $m_{T_+} \geq 2100$ GeV. Here, the value $R = 1$ corresponds to the case where minimal fine-tuning and minimal top partner mass m_{T_+} can be achieved so that this benchmark case can test the natural regions of the LHT parameter space.

In Fig. 9, we show the 2σ limit from FCC-eh with polarized e^- beams, where the limits from the indirect measurements and the LHC experiments have also been displayed. In order to examine the fine-tuning, we also show the contours of required fine-tuning 1%, 2%, and 5% in Fig. 9. To be clear, we show these limits in the $R - f$ plane (left) and $L - m_{T_+}$ plane (right) in the two different panels of Fig. 9, respectively. From the left panel of Fig. 9, we can see that there will be a considerable $R - f$ region beyond the current LHC and indirect experiments can be excluded by the FCC-eh with the integrated luminosity $L > 100$ fb^{-1}. Besides, for the same integrated luminosity of 3000 fb^{-1}, we can see that the limit ability of the FCC-eh is mildly weaker than the HL-LHC for $R < 1.5$, but better than the HL-LHC for $R > 1.5$.

In the right panel of Fig. 9, we can see that the FCC-eh can exclude the top partner mass m_{T_+} up to 1350 GeV, 1500 GeV, and 1565 GeV with integrated luminosities of 100 fb^{-1}, 1000 fb^{-1}, and 3000 fb^{-1} at the 2σ level based on the limit of the EWPO and the Higgs data. Considering the limits from the FCC-eh with 3000 fb^{-1}, which

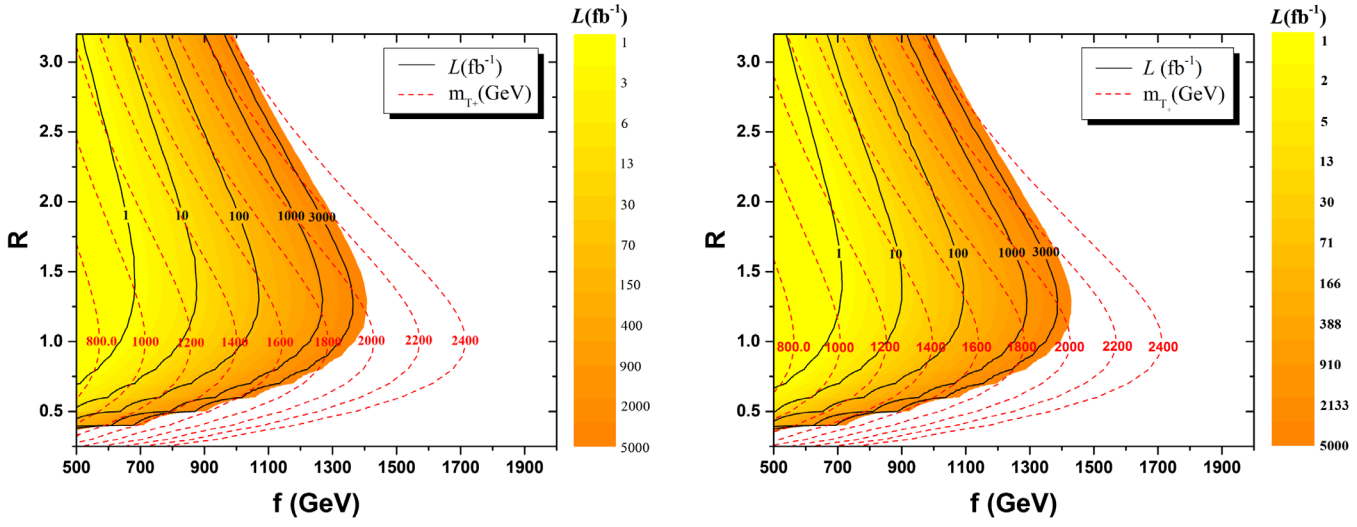

(a) FCC-eh (unPola) (b) FCC-eh (Pola)

FIG. 8. Same as Fig. 5, but for FCC-eh.

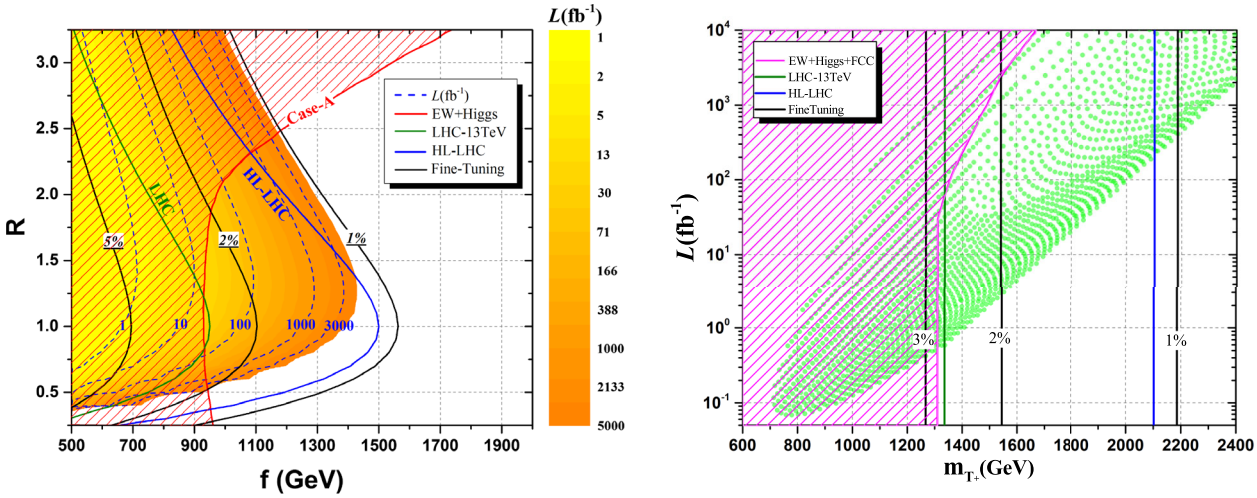

FIG. 9. (left) The 2σ limit from FCC-eh with polarized e^- beams and the 2σ limit from the EWPO and Higgs data, the LHC experiment, and the fine-tuning in the $R-f$ plane. (right) The corresponding 2σ limits in the $L-m_{T_+}$ plane.

corresponds to the top partner mass $m_{T_+} > 1565$ GeV, we can see that the allowed fine-tuning will reach 2%. If further considering the HL-LHC limit, the fine-tuning above 1% will still be allowed. However, the limit of the HL-LHC shown here is just a rough estimate, we will need full data from the HL-LHC to decide whether naturalness is actually an issue or not. As for the HE-LHC or the FCC-hh, we hope they will shed light on the exploration of new physics. So far, they are still incomplete prestudy schemes, and more motivations on the detection capability are needed.

IV. SUMMARY

In the LHT model, we investigate the single production of vectorlike top partner through $e^- p \to \nu_e \bar{T}_+ (\to \bar{b} W^-) \to \nu_e (\bar{b} \nu_l l^-) \to l^- + \bar{b} + \not{E}_T$ at the future ep colliders. We calculate the production cross sections with (un)polarized electron beams at the LHeC ($\sqrt{s} = 1.98$ TeV) and FCC-eh ($\sqrt{s} = 5.29$ TeV), respectively. In order to study the observability of this signal at the ep colliders, we perform a fast detector simulation and choose some kinematic cuts to improve the statistical significance. Besides, we find that the polarized beams can also enhance the statistical significance. For the LHeC collider, the limit on the top partner mass from the search for the T_+ in this Wb channel is weaker than the current limits from the indirect measurements and the LHC direct searches. For the FCC-eh with polarized e^- beams, we find that the top partner mass can be excluded up to 1350 GeV, 1500 GeV, and 1565 GeV with integrated luminosities of 100 fb^{-1}, 1000 fb^{-1}, and 3000 fb^{-1} at the 2σ level, which is better than the current direct and indirect searches. With the same integrated luminosity of 3000 fb^{-1}, we can see that FCC-eh and HL-LHC have different advantages in different parameter spaces, respectively. Although the allowed fine-tuning will drop to less than 2%, it is still acceptable.

ACKNOWLEDGMENTS

We thank Dr. Ruibo Li from Zhejiang University for his enthusiastic discussion and help. This work is supported by National Natural Science Foundation of China (NNSFC) (Grants No. 11405047 and No. 11305049) and the Startup Foundation for Doctors of Henan Normal University (Grant No. qd15207).

[1] ATLAS Collaboration, Phys. Lett. B **716**, 1 (2012).
[2] CMS Collaboration, Phys. Lett. B **716**, 30 (2012).
[3] L. Susskind, Phys. Rev. D **20**, 2619 (1979).
[4] H. C. Cheng and I. Low, J. High Energy Phys. 09 (2003) 051.
[5] H. C. Cheng and I. Low, J. High Energy Phys. 08 (2004) 061.
[6] I. Low, J. High Energy Phys. 10 (2004) 067.
[7] H. E. Haber and G. L. Kane, Phys. Rep. **117**, 75 (1985).
[8] ATLAS Collaboration, Phys. Rev. Lett. **121**, 211801 (2018).
[9] CMS Collaboration, Phys. Lett. B **781**, 574 (2018).
[10] See examples: M. Buchkremer, G. Cacciapaglia, A. Deandrea, and L. Panizzi, Nucl. Phys. **B876**, 376 (2013); J. Reuter and M. Tonini, J. High Energy Phys. 01 (2015) 088; N. Liu, L. Wu, B. F. Yang, and M. C. Zhang, Phys. Lett. B **753**, 664 (2016);

C. C. Han, A. Kobakhidze, N. Liu, L. Wu, and B. F. Yang, Nucl. Phys. **B890**, 388 (2015); L. Basso and J. Andrea, J. High Energy Phys. 02 (2015) 032; B. F. Yang, B. F. Hou, and H. Y. Zhang, Nucl. Phys. **B929**, 207 (2018); B. F. Yang, H. B. Shao, and J. Z. Han, Eur. Phys. J. C **78**, 184 (2018).
[11] ATLAS and CMS Collaborations, arXiv:1902.10229.
[12] Future Circular Collider Study, https://fcc.web.cern.ch/Pages/default.aspx.
[13] CEPC Study Group, arXiv:1809.00285; J. Guimaraes da Costa *et al.* (CEPC Study Group), arXiv:1811.10545.
[14] T. Barklow, J. Brau, K. Fujii, J. Gao, J. List, N. Walker, and K. Yokoya, arXiv:1506.07830; K. Fujii *et al.*, arXiv:1710.07621.
[15] CLIC Conceptual Design Report, http://project-clic-cdr.web.cern.ch/project-clic-cdr/.
[16] A. M. Cooper-Sarkar, Proc. Sci., DIS2015 (**2015**) 005 [arXiv:1507.03849].
[17] C. Schwanenberger (LHeC/FCC-eh Study Group), Proc. Sci., EPS-HEP2017 (**2018**) 464; D. Britzger and M. Klein, Proc. Sci., DIS2017 (**2018**) 105; G. Azuelos, H. Sun, and K. Wang, Phys. Rev. D **97**, 116005 (2018); Y. B. Liu, Nucl. Phys. **B923**, 312 (2017); C. C. Han, R. B. Li, R. Q. Pan, and K. Wang, Phys. Rev. D **98**, 115003 (2018).
[18] LHeC Study Group, J. Phys. G **39**, 075001 (2012).
[19] Y. C. Acar, A. N. Akay, S. Beser, A. C. Canbay, H. Karadeniz, U. Kaya, B. B. Oner, and S. Sultansoy, Nucl. Instrum. Methods Phys. Res., Sect. A **871**, 47 (2017).
[20] J. Hubisz and P. Meade, Phys. Rev. D **71**, 035016 (2005); A. Belyaev, C.-R. Chen, K. Tobe, and C.-P. Yuan, Phys. Rev. D **74**, 115020 (2006); M. Perelstein, Prog. Part. Nucl. Phys. **58**, 247 (2007).
[21] J. Reuter, M. Tonini, and M. de Vries, J. High Energy Phys. 02 (2014) 053.
[22] G. D'Ambrosio, G. F. Giudice, G. Isidori, and A. Strumia, Nucl. Phys. **B645**, 155 (2002); M. Blanke, A. J. Buras, A. Poschenrieder, S. Recksiegel, C. Tarantino, S. Uhlig, and A. Weiler, J. High Energy Phys. 01 (2007) 066.
[23] L. Wu, B. Yang, and M. Zhang, J. High Energy Phys. 12 (2016) 152.
[24] B. Yang, G. Mi, and N. Liu, J. High Energy Phys. 10 (2014) 047.
[25] D. Dercks, G. Moortgat-Pick, J. Reuter, and S. Y. Shim, J. High Energy Phys. 05 (2018) 049.
[26] Particle Data Group, Phys. Rev. D **98**, 030001 (2018).
[27] L. Shang and Y. Zhang, Easyscan_HEP, https://easyscanhep.hepforge.org.
[28] G. Moortgat-Pick *et al.*, Phys. Rep. **460**, 131 (2008).
[29] J. Alwall, M. Herquet, F. Maltoni, O. Mattelaer, and T. Stelzer, J. High Energy Phys. 06 (2011) 128.
[30] R. D. Ball *et al.*, Nucl. Phys. **B867**, 244 (2013).
[31] T. Sjostrand, S. Mrenna, and P. Z. Skands, J. High Energy Phys. 05 (2006) 026.
[32] J. de Favereau, C. Delaere, P. Demin, A. Giammanco, V. Lemaître, A. Mertens, and M. Selvaggi (DELPHES 3 Collaboration), J. High Energy Phys. 02 (2014) 057.
[33] M. Cacciari, G. P. Salam, and G. Soyez, J. High Energy Phys. 04 (2008) 063.
[34] E. Conte, B. Fuks, and G. Serret, Comput. Phys. Commun. **184**, 222 (2013).
[35] E. Conte, B. Dumont, B. Fuks, and C. Wymant, Eur. Phys. J. C **74**, 3103 (2014).
[36] G. Cowan, K. Cranmer, E. Gross, and O. Vitells, Eur. Phys. J. C **71**, 1554 (2011).
[37] B. F. Yang, H. Y. Zhang, B. F. Hou, and N. Liu, Chin. Phys. C **42**, 103102 (2018).
[38] C. R. Chen, K. Tobe, and C.-P. Yuan, Phys. Lett. B **640**, 263 (2006).